PAPER • OPEN ACCESS

Interplay between electron–electron and electron–vibration interactions on the thermoelectric properties of molecular junctions

To cite this article: C A Perroni *et al* 2015 *New J. Phys.* **17** 083050

New Journal of Physics
The open access journal at the forefront of physics

Deutsche Physikalische Gesellschaft DPG
IOP Institute of Physics

Published in partnership with: Deutsche Physikalische Gesellschaft and the Institute of Physics

OPEN ACCESS

RECEIVED
19 April 2015

REVISED
30 June 2015

ACCEPTED FOR PUBLICATION
14 July 2015

PUBLISHED
24 August 2015

PAPER

Interplay between electron–electron and electron–vibration interactions on the thermoelectric properties of molecular junctions

C A Perroni[1], **D Ninno**[1,2] **and V Cataudella**[1]

[1] CNR-SPIN and Dipartimento di Fisica, Universita' degli Studi di Napoli Federico II, Complesso Universitario Monte S. Angelo, Via Cintia, I-80126 Napoli, Italy
[2] IMAST S.c.ar.l.-Technological District on Engineering of polymeric and composite Materials and Structures, Piazza Bovio 22, I-80133 Napoli, Italy

E-mail: perroni@na.infn.it

Keywords: nanoelectronics, thermoelectricity, molecular junctions

Abstract

The linear and non-linear thermoelectric properties of molecular junctions are theoretically studied close to room temperature within a model including electron–electron and electron–vibration interactions on the molecule. A non-equilibrium adiabatic approach is devised to include a strong Coulomb repulsion and applied to the self-consistent calculation of electron and phonon transport properties of massive molecules, such as fullerenes, within the Coulomb blockade regime. We show that the phonon thermal conductance is quite sensitive to strong electron–electron interactions within the intermediate electron–vibration coupling regime. Furthermore, the electron–vibration interaction enhances both phonon and electron thermal conductance, and it reduces not only the charge conductance, but also the thermopower. The effect of the strong electron–electron interactions provides a peculiar double-peak structure to the thermopower versus charge conductance curve. Finally, within the regime of weak to intermediate electron–vibration and vibration–lead phonon coupling, the peak values of the thermoelectric figure of merit are slightly less than unity, and the maximal efficiency of the junction can reach values slightly less than half of the Carnot limit for large temperature differences between the leads.

1. Introduction

Direct conversion of temperature differences to electric voltage and vice versa can take place in solid state systems. These thermoelectric effects can be strong enough in some semiconducting materials to allow either the fabrication of devices converting wasted heat into electrical energy or the realization of solid-state coolers [1, 2]. A fundamental parameter to quantify the energy conversion efficiency is the dimensionless figure of merit $ZT = GS^2T/G_K$, where G is the electrical conductance, S the thermopower, T the absolute temperature, and $G_K = G_K^{el} + G_K^{ph}$ is the total thermal conductance, with G_K^{el} and G_K^{ph} as electron and phonon thermal conductance, respectively. Indeed, in order to improve the efficiency, mutually contrasting transport properties of the same material have to be optimized. For instance, in metals, ZT is typically limited by the Wiedemann–Franz law [3], which constrains the ratio between thermal and electric conductivities. A Large effort is currently being made in material science to get compounds with values of ZT larger than 1 and to use solid state systems for actual thermoelectric devices [1, 4, 5].

Recently, the possibility of controlling materials at the nanoscale has been exploited to optimize the thermoelectric efficiency [4, 6, 7]. For example, a maximum $ZT \simeq 2.4$ has been observed at room temperature in Bi_2Te_3/Sb_2Te_3 superlattice thermoelectric devices [8]. High values of ZT have been reported in quantum dot superlattices [9] and in semiconductor nanowires [10], where phonon confinement can lead to a lower phonon thermal conductance [11, 12]. Actually, a significant reduction in lattice thermal conductivity is considered as the main route for having high ZT in low-dimensional materials [13]. The improvement of thermoelectric efficiency can also derive from the discreteness of energy levels in nanostructures resulting into a violation of the

Wiedemann–Franz law [14]. Finally, in nanoscopic Coulomb-coupled systems, the thermoelectric properties can be optimized by exploiting the Coulomb blockade regime and changing the gate voltage [7].

Molecular devices can be efficient converters of heat into electric energy since both phonon and electron properties can contribute to an increase in the thermoelectric figure of merit ZT [15, 16]. Indeed, the emerging field of molecular thermoelectrics has attracted a lot of attention in recent years [17–23]. The thermoelectric properties of molecular junctions are also interesting in that they can provide useful information on charge and energy transport which is otherwise difficult to obtain, such as the type of carriers (electrons/holes) dominating the transport [17, 18, 24–26]. Measurements of thermoelectric properties have been performed in junctions with fullerene (C_{60}) [18] finding a high value of the molecular thermopower (S of the order of -30 μV/K). In these experiments, three different metallic electrodes (platinum, gold, and silver) have been considered achieving a more controllable alignment between the Fermi level and molecular orbitals (whose energy separation is still of the order of 0.5 eV). However, the application of a gate voltage remains elusive in these kinds of measurements. Moreover, heat transport in molecular devices remains poorly characterized due to experimental challenges [16, 27–29] or limited to a range where transport is elastic [30].

In molecular junctions, intramolecular electron–electron and electron–vibration interactions typically constitute the largest energy scales affecting the thermoelectric properties [25, 31, 32]. Moreover, the center of mass oscillation of the molecule [33], or thermally induced acoustic phonons [34] can be an additional source of coupling between electronic and vibrational degrees of freedom. The effects of intramolecular interactions on the transport properties have been studied in the regime of linear response and fully out-of-equilibrium by different theoretical tools [25, 32]. The thermopower S and the thermoelectric figure of merit ZT have been found to be sensitive to the strength of intramolecular interactions [21–23, 35–41]. However, the phonon thermal contribution G_K^{ph} to the figure of merit ZT has been calculated only at a perturbative level of the electron–vibration coupling [42].

In devices with large molecules or carbon nanotube quantum dots [43], a nonequilibrium adiabatic approach has been introduced for spinless electrons exploiting the low energy of the relevant vibrational degrees of freedom [44–48]. This method is semiclassical for the vibrational dynamics, but it is valid for arbitrary strength of electron–vibration coupling. Within this approach, we have recently implemented a self-consistent calculation for electron and phonon thermal conductance focusing only on the effects of the electron–vibration coupling for the linear response regime [49].

In this paper, we have studied the linear and non-linear thermoelectric properties of a molecular junction with electron–electron and electron–vibration interactions devising a self-consistent calculation of the electron and phonon transport properties close to room temperature. The non-equilibrium adiabatic approach has been correctly generalized to treat finite strong Coulomb interactions within a junction model which takes into account the interplay between the low frequency center of mass oscillation of the molecule and the electronic degrees of freedom within the Coulomb blockade regime. Parameters appropriate for junctions with C_{60} molecules are considered. We have found that, within the intermediate electron–vibration coupling regime, the effects of electron–electron interactions can enhance G_K^{ph}, which acquires an order of magnitude and a behavior similar to that of electron thermal conductance as a function of the gate voltage. The electron–vibration interaction induces an increase of the phonon and electron thermal conductance, and a decrease of not only the charge conductance, but also of the thermopower. The effect of the strong electron–electron interactions provides a peculiar double–peak structure to the S versus charge conductance G curve. The overall effect of the electron–electron and electron–vibration interactions induces a reduction of the thermoelectric figure of merit ZT, which, however, within the regime of weak to intermediate electron–vibration and vibration-lead phonon coupling, can have peak values slightly less than unity. Finally, within the non-linear response regime, the efficiency can be correlated to the behavior of ZT as a function of the gate voltage, and it is found to be slightly less than half of the Carnot limit within the regime of weak to intermediate electron–vibration and lead phonon–vibration coupling.

The paper is organized as follows. In section 2, the model of molecular junction is proposed. In section 3, the adiabatic approach generalized for strong local Coulomb interactions is explained. In sections 4 and 5, the results within the linear and nonlinear regime, respectively, are discussed. The paper is closed by appendix A, where the comparison between different treatments of the large Coulomb repulsion is made within the Coulomb blockade regime, and by appendix B, where the transport properties are analyzed for different values of the electron–electron interaction.

2. Molecular junction model

In this paper, we describe the molecular junction within the Anderson–Holstein model, which is a reference for these devices although it has no exact solution [25, 50]. The molecule is modeled as a single electronic level

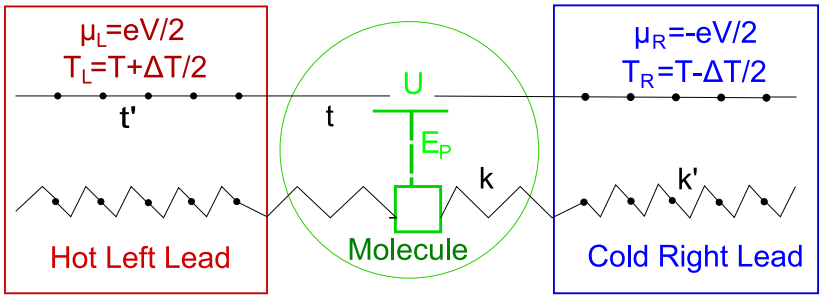

Figure 1. Sketch of the molecular junction studied in this work. The straight lines between dots (lead atoms) depict charge electron hoppings in the lead bulks (t') and between lead and molecule (t). The broken lines between dots (lead atoms) depict springs in the lead bulks (with elastic constant k') and between lead and molecule (with elastic constant k). The hot left lead and the cold right lead are kept at chemical potential $\mu_L = eV/2$, temperature $T_L = T + \Delta T/2$ and chemical potential $\mu_R = -eV/2$, temperature $T_R = T - \Delta T/2$, respectively, with e modulus of the electron charge, V bias potential, $\mu = 0$ average chemical potential, T average temperature. The term U indicates the presence of electron–electron interactions, while the term E_P indicates electron–vibration interactions on the molecule.

locally interacting with a single vibrational mode. In addition to the electron–vibration coupling, electrons with opposite spins can locally interact through a Coulomb Hubbard term (see figure 1 for a sketch of the molecular junction model).

The Hamiltonian $\hat{H}$ is given by

$$\hat{H} = \hat{H}_{el} + \hat{H}_{ph} + \hat{H}_{\rm int}, \tag{1}$$

where the Hamiltonian $\hat{H}_{el}$ takes into account the electronic degrees of freedom of the leads and the molecule, $\hat{H}_{ph}$ the vibrational degrees of freedom of the leads and the molecule, and $\hat{H}_{\rm int}$ the coupling between electronic and vibrational degrees of freedom.

The electronic Hamiltonian $\hat{H}_{el}$ of equation (1) is

$$\hat{H}_{el} = \epsilon \sum_{\sigma} \hat{n}_{\sigma} + U \hat{n}_{\uparrow} \hat{n}_{\downarrow} + \sum_{q,\alpha,\sigma} \varepsilon_{q,\alpha} \hat{n}_{q,\alpha,\sigma} + \sum_{q,\alpha,\sigma} \left(V_{q,\alpha} \hat{c}^{\dagger}_{q,\alpha,\sigma} \hat{d}_{\sigma} + h.\,c. \right), \tag{2}$$

where the molecular electronic level has energy ϵ, the σ spin electron density operator is $\hat{n}_{\sigma} = \hat{d}^{\dagger}_{\sigma} \hat{d}_{\sigma}$, with $\hat{d}^{\dagger}_{\sigma}$ ($\hat{d}_{\sigma}$) creation (annihilation) σ spin electron operator on the molecule. The presence of a gate in the junction can be simply simulated by changing the value of the local energy ϵ [25]. The Coulomb repulsion on the molecule is simulated with a Hubbard term U, which gives an energy penalty for electron occupations with spin $\uparrow$ and $\downarrow$ [25]. The lead density operator is $\hat{n}_{q,\alpha,\sigma} = \hat{c}^{\dagger}_{q,\alpha,\sigma} \hat{c}_{q,\alpha,\sigma}$, where the operators $\hat{c}^{\dagger}_{q,\alpha,\sigma}$ ($\hat{c}_{q,\alpha,\sigma}$) create (annihilate) electrons with momentum q, spin σ, and energy $\varepsilon_{q,\alpha} = \xi_{q,\alpha} - \mu_{\alpha}$ in the left ($\alpha = L$) or right ($\alpha = R$) free metallic leads, with μ_{α} chemical potential of the lead α in equilibrium at the temperature T_{α}. We consider the temperatures $T_L = T + \Delta T/2$ and $T_R = T - \Delta T/2$, with T average temperature. Moreover, we fix the chemical potentials $\mu_L = eV/2$ and $\mu_R = -eV/2$, with e modulus of the electron charge, V bias potential, and average chemical potential $\mu = 0$. The electronic tunneling between the molecular dot and a state q in the lead α has the amplitude $V_{q,\alpha}$. As usual for metallic leads, the density of states $\rho_{q,\alpha}$ is assumed flat around the small energy range relevant for the molecular orbital, making valid the wide-band limit $\rho_{q,\alpha} \mapsto \rho_{\alpha}$, $V_{q,\alpha} \mapsto V_{\alpha}$. Therefore, the full hybridization width of the molecular orbital is $\hbar\Gamma = \sum_{\alpha} \hbar\Gamma_{\alpha}$, with $\hbar$ the Planck constant and the tunneling rate $\Gamma_{\alpha} = 2\pi\rho_{\alpha} |V_{\alpha}|^2/\hbar$. In the following, we consider the symmetric configuration: $\Gamma_L = \Gamma_R = \Gamma/2$.

In equation (1), the Hamiltonian $\hat{H}_{ph}$ describes the vibrations of the slow mode (focus will be on the center of mass mode), the free phonon modes of the leads, and the coupling between them:

$$\hat{H}_{ph} = \hat{H}_{cm} + \sum_{q,\alpha} \hbar\omega_{q,\alpha} \hat{a}^{\dagger}_{q,\alpha} \hat{a}_{q,\alpha} + \sum_{q,\alpha} \left(C_{q,\alpha} \hat{a}_{q,\alpha} + h.\,c. \right) \hat{x}. \tag{3}$$

The center of mass Hamiltonian $\hat{H}_{cm}$ is

$$\hat{H}_{cm} = \frac{\hat{p}^2}{2M} + \frac{k\hat{x}^2}{2}, \tag{4}$$

where $\hat{p}$ and $\hat{x}$ are the center of mass momentum and position operators, respectively, M is the total large mass, k is the effective spring constant, with frequency $\omega_0 = \sqrt{k/M}$. In equation (3), the operators $\hat{a}^{\dagger}_{q,\alpha}$ ($\hat{a}_{q,\alpha}$) create (annihilate) phonons with momentum q and frequency $\omega_{q,\alpha}$ in the lead α. The left and right phonon leads will be

considered as thermostats in equilibrium at the same temperatures T_L and T_R, respectively, of the electron leads. Finally, in equation (3), the coupling between the center of mass position and a phonon q in the lead α is given by the elastic constant $C_{q,\alpha}$. For large molecules, the center of mass mode has a low frequency ω_0 which is typically smaller than the Debye frequency ω_D of the metallic leads ($\hbar\omega_D \simeq 15 - 20$ meV for metals like silver, gold, and platinum [3]). Therefore, for large molecules, the adiabatic regime is valid for the center of mass oscillator $\omega_0 \ll \Gamma$ and $\omega_0 \ll \omega_D$. Within this regime, the effect of the α phonon lead on the center of mass mode provides a constant damping rate γ_α [51]. In analogy with the electronic dynamics, we consider the symmetric configuration: $\gamma_L = \gamma_R = \gamma/2$.

Finally, the interaction term $\hat{H}_{\rm int}$ in the Anderson–Holstein model of equation(1) is provided by a linear coupling between the total electron density on the molecule, $\hat{n} = \sum_\sigma \hat{n}_\sigma$, and the $\hat{x}$ operator of the center of mass:

$$\hat{H}_{\rm int} = \lambda \hat{x} \hat{n}, \tag{5}$$

where λ is the electron–vibration coupling constant. In the following, the electron–vibration interaction will be described in terms of the coupling energy $E_P = \lambda^2/(2k)$.

In this work, we analyze a simple model for the vibrational degrees of freedom. We do not consider molecular internal modes since we expect that, in comparison with the center of mass mode, they are much less coupled to the phonon leads (the strength of the interaction between molecular vibrations and lead phonons will be a relevant quantity in our analysis). In any case, the overall effects of a more realistic vibrational system are consistent with our results confirming that the phonon contribution to the total thermal conductance can be relevant [52]. Moreover, the focus of this paper is on the regime close to room temperature; therefore we neglect possible but negligible phonon interference effects [53].

We will consider model parameters appropriate to junctions with C_{60} molecules following the analysis reported in a previous paper [49]. In these molecular junctions, attention can be focused on a molecular electronic orbital which is sufficiently separated in energy from other orbitals [49, 54–56]. The hybridization width $\hbar\Gamma$ of the orbital has been estimated to be of the order of 20 meV [55, 56]. Even if the local Coulomb repulsion is reduced by the screening of the electrodes, the energy U is expected to be at least one order of magnitude larger than $\hbar\Gamma$ [55, 56]. The center of mass mode can be considered as the relevant vibrational mode of the C_{60} molecular junction [49]. Indeed, experiments have evidenced a coupling between the center of mass mode and the electron dynamics in these junctions [33]. In these experiments, $\hbar\omega_0$ has been estimated to be of the order of 5 meV [33], hence $\omega_0 \simeq 0.25\ \Gamma$. Finally, for junctions with C_{60} molecules and leads of Ag, Au, and Pt, $\hbar\gamma \simeq 3 - 8$ meV, therefore γ is of the same order of ω_0 ($\gamma \simeq 0.15 - 0.40\ \Gamma$) [49].

In this paper, $\hbar\Gamma \simeq 20$ meV will be the energy unit (Γ the frequency unit, $1/\Gamma$ the time unit). We will measure lengths in units of $2\lambda/k$, and temperatures in units of $\hbar\Gamma/k_B$, with k_B as the Boltzmann constant (the room temperature is of the order of 1.25 in these units).

3. Adiabatic approach within the Coulomb blockade regime

The focus of this paper is on charge and heat transport properties close to room temperature, therefore for parameters appropriate to the Coulomb blockade regime: $\hbar\omega_0 \ll \hbar\omega_D \simeq \hbar\Gamma \leqslant k_B T \ll U$, with $U > 10\ \hbar\Gamma$. Besides, the electron–vibration coupling is not weak, but it is estimated to be in the intermediate regime, i.e. $\hbar\omega_0 \leqslant E_P \simeq \hbar\Gamma$. Since $\hbar\omega_0$ is the lowest energy scale, the dynamics of the slow center of mass can be treated as classical. In the following, the position and the momentum of the oscillator will be indicated by the c-numbers x and p, respectively. The parameter regime appropriate to these junctions requires a generalization of the adiabatic approach to the physical situation where the Coulomb interaction is finite and large. Recently, the adiabatic approach has been combined with a treatment of electron–electron interactions within a slave–boson approach [57] which is valid only in the limit of infinite local Coulomb repulsion for energies close to the chemical potential and low temperatures [58].

3.1. Electron dynamics at a fixed value of the oscillator displacement

The electronic dynamics turns out to be equivalent to that of an adiabatically slow level with energy $E_0(t) = \epsilon + \lambda x(t)$ within the Coulomb blockade regime [59, 60].

At the zero order of the adiabatic expansion, the electronic quantities can be calculated considering an energy level with a fixed oscillator position x. The effects of the strong Coulomb repulsion are treated by inserting the first self-energy correction upon the atomic limit [50]. Therefore, for the paramagnetic solution, the level spectral function $A_0(\omega, x)$ at zero order of the adiabatic expansion becomes

$$A_0(\omega, x) = [1 - \rho(x)]\frac{\hbar\Gamma}{(\hbar\omega - \epsilon - \lambda x)^2 + (\hbar\Gamma)^2/4} + \rho(x)\frac{\hbar\Gamma}{(\hbar\omega - \epsilon - \lambda x - U)^2 + (\hbar\Gamma)^2/4}, \quad (6)$$

where $\rho(x)$ is the level density per spin self-consistently calculated at fixed position x through the following integral

$$\rho(x) = \int_{-\infty}^{+\infty} \frac{\mathrm{d}(\hbar\omega)}{2\pi i} G_0^<(\omega, x), \quad (7)$$

with the lesser Green function $G_0^<(\omega, x)$

$$G_0^<(\omega, x) = \frac{i}{2}\Big[f_L(\omega) + f_R(\omega)\Big]A_0(\omega, x), \quad (8)$$

and $f_\alpha(\hbar\omega) = 1/(\exp[\beta_\alpha(\hbar\omega - \mu_\alpha)] + 1)$ Fermi distribution of the lead α ($\beta_\alpha = 1/k_B T_\alpha$). Actually, the spectral function is characterized by a double-peak structure that, for large U, is robust against the effects of electron–vibration coupling which tend to shift and enlarge the single peaks (the single-peak width increases by a factor of the order of E_P).

In appendix A, we compare the spectral function of this treatment for strong Coulomb repulsion with that of another approach which retains additional self-energy corrections upon the atomic limit in the absence of electron–vibration coupling [50]. For large U and room temperature, the approach considered here is very accurate, therefore, it represents an optimal starting point for the adiabatic expansion. In this paper, we will study different properties varying the electronic level occupation. In our model, these variations can be controlled by changing the molecule level energy ϵ with respect to the lead's chemical potential (average chemical potential $\mu = 0$ in this work). In appendix A, we report the molecular electron occupation N as a function of level energy ϵ showing the typical profiles of the Coulomb blockade. In particular, the following energies are relevant: $\epsilon = -U/2$ (close to half-filling $N = 1$), $\epsilon = -U$ (transition from level occupation $N = 1$ to $N = 2$), $\epsilon = 0$ (from level occupation $N = 1$ to $N = 0$).

Within the adiabatic approach, one can determine the electronic Green functions and other electronic quantities making an expansion on the small oscillator velocity $v = p/m$. In the absence of electron–electron interactions, the adiabatic expansion can be determined for any strength of electron–vibration coupling [47, 48, 61–63]. In this paper, an approach is devised for the case of strong Coulomb repulsion in order to include the effects of electron–vibration interaction within the realistic intermediate coupling regime. Actually, the approach used in this paper is valid as long as the two peaks characteristic of Coulomb blockade can be resolved, therefore for the physical regime $E_P \ll U$. In the next subsection, we will use the adiabatic expansion of the level occupation to derive the motion equation of the slow center of mass oscillator in a self-consistent way.

3.2. Dynamics of the center of mass oscillator

The effect of the molecule electron degrees of freedom and of the phonon baths in the leads gives rise to the following generalized Langevin equation for the slow center of mass variable

$$m\frac{\mathrm{d}v}{\mathrm{d}t} = F_{\mathrm{det}}(x, v) + \xi(x, t), \quad (9)$$

which contains the deterministic force $F_{\mathrm{det}}(x, v)$ and the position dependent fluctuating force $\xi(x, t)$. The deterministic force

$$F_{\mathrm{det}}(x, v) = F_{\mathrm{gen}}(x) - A_{\mathrm{eff}}(x)v, \quad (10)$$

can be decomposed into a generalized force $F_{\mathrm{gen}}(x)$

$$F_{\mathrm{gen}}(x) = -kx + F_\lambda(x), \quad (11)$$

with $F_\lambda(x) = -2\lambda\rho(x)$ induced by the electron–vibration coupling, and, as a result of the adiabatic expansion, a dissipative force with an effective position dependent positive definite term $A_{\mathrm{eff}}(x)$

$$A_{\mathrm{eff}}(x) = A_\lambda(x) + m\gamma, \quad (12)$$

with $A_\lambda(x)$

$$A_\lambda(x) = 2\hbar\lambda^2 \int_{-\infty}^{+\infty} \frac{\mathrm{d}(\hbar\omega)}{2\pi i} G_0^<(\omega, x)\left[\frac{\partial A_0(\omega, x)}{\partial(\hbar\omega)}\right] \quad (13)$$

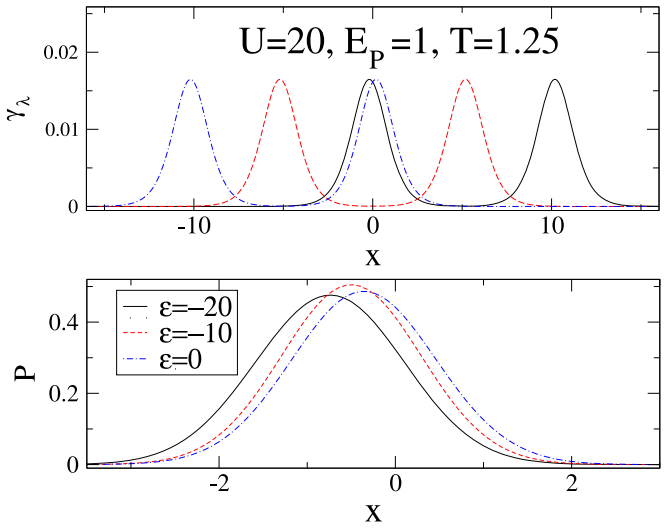

Figure 2. Electron–vibration induced damping rate γ_λ in units of Γ (upper panel) and reduced position distribution function P in units of $k/2\lambda$ (lower panel) as a function of oscillator position x (in units of $2\lambda/k$) for different values of level energy ϵ (in units of $\hbar\Gamma$). In all the plots, $U = 20\hbar\Gamma$, $E_P = \hbar\Gamma$, and temperature $T = 1.25\hbar\Gamma/k_B$ (close to room temperature).

due to the electron–vibration interaction. The fluctuating force $\xi(x, t)$ in equation (9) is such that

$$\langle \xi(x, t) \rangle = 0, \qquad \langle \xi(x, t)\xi(x, t') \rangle = D_{\rm eff}(x)\delta(t - t'), \tag{14}$$

where the effective position dependent noise term $D_{\rm eff}(x)$ is

$$D_{\rm eff}(x) = D_\lambda(x) + k_B\Big(T_L + T_R\Big)m\gamma, \tag{15}$$

with $D_\lambda(x)$

$$D_\lambda(x) = 2\hbar\lambda^2 \int_{-\infty}^{+\infty} \frac{{\rm d}(\hbar\omega)}{2\pi i} G_0^<(\omega, x) G_0^>(\omega, x) \tag{16}$$

determined by the electron–vibration coupling and the greater Green function $G_0^>(\omega, x)$

$$G_0^>(\omega, x) = -\frac{i}{2}\Big[2 - f_L(\omega) - f_R(\omega)\Big]A_0(\omega, x). \tag{17}$$

It is worthwhile pointing out that, in equilibrium conditions at temperature $T = T_\alpha$ and chemical potential $\mu = \mu_\alpha = 0$, the adiabatic procedure gives rise to a generalized fluctuation–dissipation relation $D_{\rm eff}(x) = 2k_B T A_{\rm eff}(x)$ valid for each fixed position x.

The solution of the Langevin equation (9) represents a central step for this work. This equation has been numerically solved under generic non-equilibrium conditions using a generalized Runge–Kutta algorithm [47, 64, 65]. As a result of the numerical calculations, the oscillator distribution function $Q(x, v)$ and the reduced position distribution function $P(x)$ are determined allowing us to evaluate static quantities relative to the center of mass oscillator. Moreover, averaging over $P(x)$ or $Q(x, v)$ will allow us to extract the mean value of any electronic observable $O(x, v)$ dependent on the oscillator parameters.

Before discussing the results (section 4), we devote the last part of this section to describing the features of the electron–vibration induced damping rate $\gamma_\lambda(x) = A_\lambda(x)/m$, with $A_\lambda(x)$ given in equation (13). We observe that the magnitude of $\gamma_\lambda(x)$ always gets enhanced with increasing the electron–vibration coupling E_P. However, as reported in the upper panel of figure 2, even for the intermediate coupling $E_P = 1$, the peak values of $\gamma_\lambda(x)$ are always smaller than the realistic values of the lead-induced damping rate γ ($\gamma = 0.15$ will be considered in this paper). This implies that the effects due to the electron–vibration coupling on the oscillator dynamics do not typically represent a large perturbation with respect to those induced by the coupling to phonon leads. Obviously, as reported in the figure, the behavior of $\gamma_\lambda(x)$ strongly depends on the occupation of the electronic level. We point out that, in contrast to the spinless case analyzed in a recent paper, [49] $\gamma_\lambda(x)$ shows a double-peak behavior due to the effect of the strong Hubbard interaction. Moreover, as reported in the upper panel of figure 2, the peaks of $\gamma_\lambda(x)$ largely shift passing from the quasi half-filling case (close to $\epsilon = -10 = -U/2$, state with flat occupation) to conditions out of half-filling (close to $\epsilon = -20 = -U$ and $\epsilon = 0 = \mu$, state with strong density fluctuations). The self-consistent calculation of $\gamma_\lambda(x)$ provides a direct signature of the strong local interaction since it is determined by the adiabatic expansion of the electron occupation.

A comparison of the x dependence between $\gamma_\lambda(x)$ and the calculated oscillator position distribution $P(x)$ will clarify the conditions under which the electron–vibration interaction can affect the dynamics of the center of mass oscillator. In the lower panel of figure 2, we report the distribution $P(x)$ with varying the level energy ϵ. We notice that, apart from the shift of the peaks, close to room temperature, the distribution $P(x)$ is practically the Gaussian of the free harmonic oscillator at temperature T for any value of the level energy ϵ. In the quasi half-filled case ($\epsilon = -10$), the peak positions of $\gamma_\lambda(x)$ and $P(x)$ are well separated. Therefore, one expects that, in this regime, the effects of the electron–vibration coupling on the oscillator dynamics are weak. We stress that, within the self-consistent procedure used in this work, the peak of the $P(x)$ directly signals that the level occupation is close to $-N/2$ within the units used in this paper. Actually, for $\epsilon = -10$, the value close to -0.5 of the peak of $P(x)$ is fully compatible with the half-filled case $N = 1$. On the other hand, for $\epsilon = -20$, the peak position of $P(x)$ shifts towards lower values close to -0.75 ($N \simeq 1.5$), and, for $\epsilon = 0$, to 0.25 ($N \simeq 0.5$). We point out that, for $\epsilon = -20$, the first peak of $\gamma_\lambda(x)$ is close to $x = 0$, while, for $\epsilon = 0$, the second peak of $\gamma_\lambda(x)$ strongly overlaps with the position distribution $P(x)$. Therefore, out of half-filling, the effects of the electron–vibration coupling can affect the oscillator dynamics. In contrast with the spinless case [49], these effects are present not only close to $\epsilon = \mu = 0$, but also to $\epsilon = -U = -20$, as a result of the strong Coulomb interaction. Therefore, as discussed in detail in the next section, the complex interplay between electron–electron and electron–vibration interactions opens an entire energy region where the phonon heat transport can be enhanced.

4. Results within the linear response regime

In this section, we will discuss linear response transport properties in an attempt to clarify the role of the electron–electron and electron–vibration interactions. In the next subsections, we will analyze the phonon heat transport, the electronic spectral function, the charge and electronic heat transport, and thermoelectric figure of merit. In the following, we will assume $\omega_0 = 0.25\Gamma$, and $\gamma = 0.15\Gamma$ (larger values of γ were discussed in a previous paper [49] for spinless electrons and they will be considered in the next section about non-equilibrium properties).

4.1. Phonon heat transport

In this subsection, we will focus on the phonon thermal conductance G_K^{ph} calculated within the linear response regime around temperature T as

$$G_K^{ph} = \lim_{\Delta T \to 0^+} \frac{\left(J_L^{ph} - J_R^{ph}\right)}{2\Delta T}, \tag{18}$$

with J_α^{ph} current from the α phonon lead [49, 66]. This quantity is directly calculated by the stochastic dynamics.

In the limit where the electron–vibration coupling E_P is weak, the resulting Langevin equation (9) is linear (all the coefficient dependencies on the position x can be disregarded) [49]. In this limit, the J_α^{ph} current can be obtained starting from the Landauer–Caroli formula

$$J_\alpha^{ph} = \frac{1}{\pi}\int_0^\infty \hbar\omega \Big[D^R(\omega) g_L(\omega) D^A(\omega) g_R(\omega) \Big] N_\alpha(\omega), \tag{19}$$

where $D^R(\omega)$ ($D^A(\omega)$) is the retarded (advanced) phononic Green function, $g_\alpha(\omega) = 2\omega\gamma_\alpha$, and $N_\alpha(\omega) = 1/(\exp(\beta_\alpha\hbar\omega) - 1)$ is the Bose distribution relative to the lead α (in this paper we will consider the appropriate high temperature limit of this distribution) [66].

The conductance G_K^{ph} is expected to be mostly sensitive to the coupling of the center of mass mode to the phonons of metallic leads through the damping rate γ ($\gamma = 0.15\Gamma$ in this work) which is typically larger than the peak values of electron–vibration induced damping rate $\gamma_\lambda(x)$. As shown in figure 3, in the regime of weak electron–vibration coupling E_P, low level occupation ($\epsilon \gg 0$), and double level occupation ($\epsilon \ll -U$), G_K^{ph} is close to $0.04\, k_B\Gamma$ ($k_B\Gamma$ is about 419.8 pW/K for $\hbar\Gamma \simeq 20$ meV), a numerical value coincident with an analytical estimate of G_K^{ph} given in a recent paper [49]. This asymptotic value corresponds to the contribution given by the only phonon leads neglecting the effects of electron–electron and electron–vibration interactions on the molecule.

In figure 3, we show that G_K^{ph} always gets larger with increasing the electron–vibration coupling E_P. Moreover, this increase of G_K^{ph} strongly depends on the value of level energy ϵ. In contrast with the spinless case (reported for comparison in figure 3 at $E_P = 1$), we stress that the enhancement of G_K^{ph} takes place not only close to $\epsilon \simeq 0$, but also to $\epsilon \simeq -U$. Therefore, the distance between the peaks of the phonon thermal conductance is controlled by the energy scale U. The peak values are almost coincident (although slightly smaller than the peak value of the spinless case), and, at $E_P = 1$, they are of the order of $0.05 k_B\Gamma \simeq 20$ pW/K. Therefore, the calculated

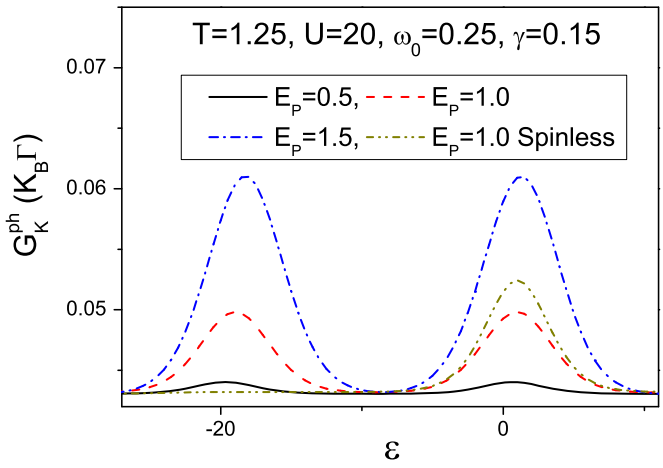

Figure 3. Phonon thermal conductance G_K^{ph} (in units of $k_B\Gamma$) as a function of the level energy ϵ (in units of $\hbar\Gamma$) for different values of electron–vibration coupling E_P (in units of $\hbar\Gamma$). In the plot, $U = 20\hbar\Gamma$, $T = 1.25\hbar\Gamma\ k_B$ (close to room temperature), $\omega_0 = 0.25\Gamma$, and oscillator damping rate $\gamma = 0.15\Gamma$.

G_K^{ph} is in very good agreement with the thermal conductance of the order of a few 10 pW/K measured for molecules anchored to gold [28, 29]. In any case, due to the strong electron–electron interactions, G_K^{ph} can be enhanced in a new large-energy region. On the other hand, for $\epsilon \simeq -U/2$, G_K^{ph} is poorly influenced by the electron–vibration effects even if E_P is not small, resulting in a value close to the asymptotic one. From this analysis emerges that the complex enhancement of the phonon thermal conductance G_K^{ph} as a function of the electron–electron and electron–vibration interactions can be mostly ascribed to the properties of additional electron–vibration induced damping rate $\gamma_\lambda(x)$ discussed in the previous section.

4.2. Electronic spectral function

From the solution of the Langevin equation, one can obtain the mean values of the relevant electronic observables, $O(x, v)$, taking the average over the oscillator distribution function. First, we discuss the features of the electronic spectral function which is at the basis of the thermoelectric properties analyzed in the next subsection.

The electronic spectral function $A(\omega)$ is evaluated making the average of the function $A_0(\omega, x)$ in equation (6) over $P(x)$:

$$A(\omega) = \int_{-\infty}^{+\infty} \mathrm{d}x P(x) A_0(\omega, x). \tag{20}$$

In this section, the spectral function will be discussed in equilibrium conditions at temperature T ($V = 0$ and $\Delta T = 0$). We recall that, in appendix A, the features of the spectral function are discussed in the absence of electron–vibration coupling. Actually, the spectral function is characterized by a structure with two peaks separated by an energy of the order of U, and it is strongly dependent on the value of the level energy ϵ.

In this subsection, we analyze the behavior of the spectral function with varying the electron–vibration coupling E_P at a fixed value of Hubbard energy U. In the upper panel of figure 4, we show the spectral function for different values of the electron–vibration coupling in the half-filled case $\epsilon = -8 = -U/2$ (level occupation $N = 1$). For comparison, we report the spectral function relative to the case where electron–electron and electron–vibration interactions are neglected (indicated as 'Free' in the figure). We point out that there is a strong transfer of spectral weight for the double-peak structure toward low frequencies with increasing E_P. In addition to the shifts of the peaks, the electron–vibration coupling tends to reduce the height of the peaks and to enlarge them. Actually, the single peaks increase their width by a factor of the order of E_P. We stress that, for realistic values of the coupling E_P, the two Hubbard peaks do not overlap, therefore the double-peak structure due to the large U is quite robust to the effects of electron–vibration coupling. Finally, we notice that, in the spinless case (reported for comparison in figure 4 at $E_P = 0.5$), the spectral function has a single peak, and it is quite sensitive to the effects of the electron–vibration coupling.

As shown in the lower panel of figure 4, a different behavior takes place in the regime of low-level occupation ($\epsilon = 8$ in the figure). For the considered values of E_P, the spectral function gets enlarged, but its peak position is quite rigid. Moreover, the differences with the spinless case are completely negligible. Even in the presence of electron–vibration coupling E_P, the behavior of the spectral function is different in the regime of half-filling and of low- or high-level occupation.

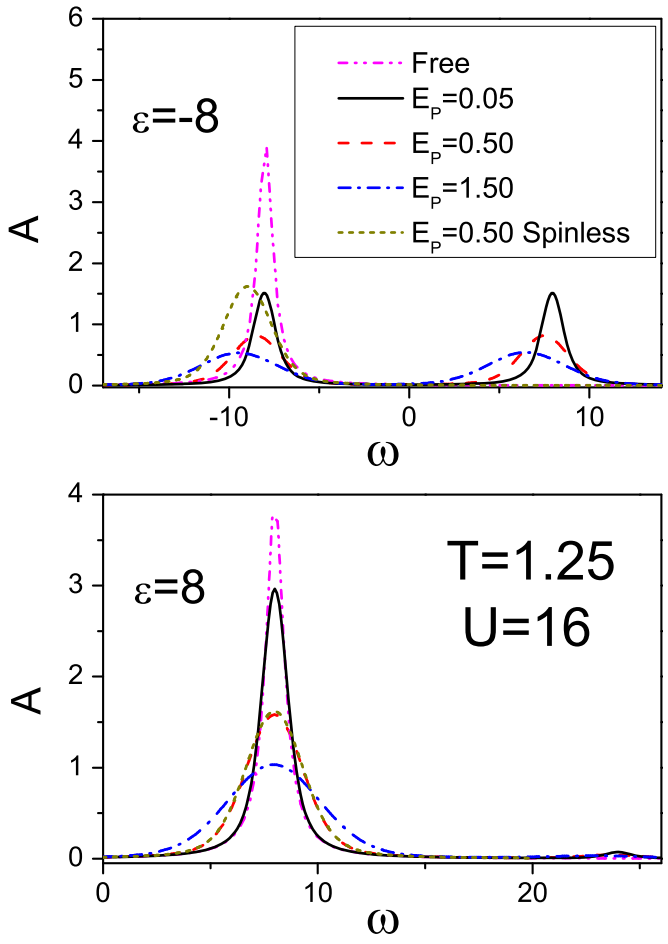

Figure 4. Spectral function (in units of $1/\hbar\Gamma$) as a function of frequency ω (in units of Γ) at level energy $\epsilon = -8\hbar\Gamma$ (upper panel) and $\epsilon = 8\hbar\Gamma$ (lower panel) for different values of E_P (in units of $\hbar\Gamma$). In all the plots, $U = 16\hbar\Gamma$, $T = 1.25\hbar\Gamma/k_B$ (close to room temperature).

4.3. Charge and electronic heat transport, and thermoelectric figure of merit

In this subsection, the focus will be on the regime of the linear response around the average chemical potential $\mu = 0$ and temperature T ($\Delta T \to 0^+$, $V \to 0^+$). We will evaluate the electronic conductance G

$$G = \left(\frac{2e^2}{\hbar}\right)\left(\frac{\hbar\Gamma}{4}\right)\int_{-\infty}^{+\infty}\frac{\mathrm{d}(\hbar\omega)}{2\pi}A(\omega)\left[-\frac{\partial f(\hbar\omega)}{\partial(\hbar\omega)}\right], \tag{21}$$

where $f(\hbar\omega) = 1/(\exp[\beta(\hbar\omega - \mu)] + 1)$ is the free Fermi distribution corresponding to the average chemical potential $\mu = 0$. Then, we will calculate the Seebeck coefficient $S = -G_S/G$, with

$$G_S = \left(\frac{2e}{\hbar}\right)\left(\frac{\hbar\Gamma}{4T}\right)\int_{-\infty}^{+\infty}\frac{\mathrm{d}(\hbar\omega)}{2\pi}(\hbar\omega)A(\omega)\left[-\frac{\partial f(\hbar\omega)}{\partial(\hbar\omega)}\right]. \tag{22}$$

Finally, we will determine the electron thermal conductance $G_K^{el} = G_Q + TG_S S$, with

$$G_Q = \left(\frac{2}{\hbar T}\right)\left(\frac{\hbar\Gamma}{4}\right)\int_{-\infty}^{+\infty}\frac{\mathrm{d}(\hbar\omega)}{2\pi}(\hbar\omega)^2A(\omega)\left[-\frac{\partial f(\hbar\omega)}{\partial(\hbar\omega)}\right]. \tag{23}$$

The total thermal conductance $G_K = G_K^{el} + G_K^{ph}$ makes feasible the evaluation of the figure of merit $ZT = GS^2T/G_K$. When the coupling of the center of mass mode to the metallic leads is absent ($\gamma = 0$), $G_K = G_K^{el}$, so that $ZT = ZT^{el}$, which can be used to characterize the electronic thermoelectric efficiency.

As reported in figure 5, we analyze the effects of the electron–vibration coupling on the electronic response functions as a function of the level energy ϵ at a fixed value of Hubbard interaction U ($U = 20$) in the absence of coupling to phonon leads ($\gamma = 0$) close to room temperature ($T = 1.25$). For comparison, we report the transport properties relative to the case when electron–electron and electron–vibration interactions are neglected (indicated as 'Free' in the figure).

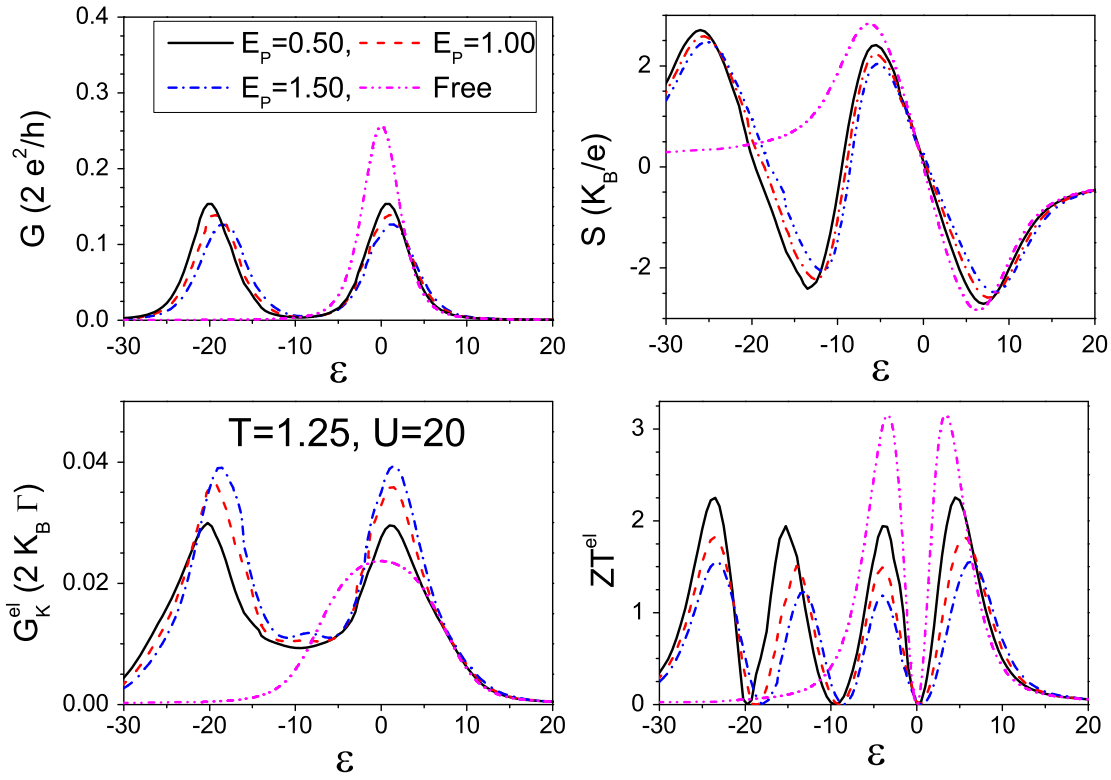

Figure 5. Electron conductance G in units of $2e^2/h$ (upper left panel), Seebeck coefficient S in units of k_B/e (upper right panel), electron thermal conductance G_K^{el} in units of $2k_B\Gamma$ (lower left panel), and figure of merit ZT^{el} (lower right panel) as a function of the level energy ϵ (in units of $\hbar\Gamma$) for different values of electron–vibration E_P (in units of $\hbar\Gamma$). In all the plots, $U = 20\hbar\Gamma$, $\gamma = 0$, and $T = 1.25\hbar\Gamma/k_B$ (close to room temperature).

The charge conductance G is expected to be smaller than the free one due to the effects of interactions. As shown in the upper left panel of figure 5, close to room temperature, G has peak values of the order of $10^{-1}\ e^2/h$ (e^2/h is about 3.87×10^{-5} S). In particular, for $\epsilon \simeq 20$, we have checked that G is of the order of $10^{-3}\ e^2/h$ in agreement with the order of magnitude of experimental data in C_{60} [18]. As expected, the conductance as a function of the level energy ϵ follows a behavior similar to the double-peak structure of the spectral function as a function of the frequency. Therefore, G has maxima for $\epsilon \simeq 0 = \mu$ and $\epsilon \simeq -U$, and a minimum at $\epsilon \simeq -U/2$.

As shown in the upper right panel of figure 5, the Seebeck coefficient S shows large variations with changing ϵ. Indeed, S shows two maxima and two minima whose magnitude is very large at room temperature being of the order of $2\ k_B/e$ (k_B/e is about 86 μeV/K). This complex behavior is due to the role played by the strong electron correlations [38]. Actually, the structure close to $\epsilon = 0$ (where S vanishes) is nearly translated by $-U$ (for $\epsilon \simeq -20$, S goes again to zero). Therefore, even at $\epsilon \simeq -U/2$, S gets very small values. Obviously, for large positive values of ϵ, S is small and negative (n-type behavior). In particular, for $\epsilon = 20$, S is about $-0.45k_B/e \simeq -38.5\mu$ V/K in agreement with the magnitude of experimental data in C_{60} [18].

As shown in the upper panels of figure 5, the most relevant effect of the coupling E_P on the conductance G and the Seebeck coefficient S is to shift the curves and reduce the magnitude of the response function. The shift of the conductance peaks and of the zeroes of the Seebeck coefficient is of the order of E_P. At fixed level energy, unlike the conductance G, the Seebeck coefficient is more sensitive to the changes of the coupling E_P. For example, this occurs for energies close to the minima and the maxima. By changing the values of ϵ, there is an inversion in the behavior of S with increasing the electron–vibration coupling E_P.

As shown in the lower left panel of figure 5, with varying the level energy ϵ, the electron thermal conductance G_K^{el} shows the characteristic double-peak structure due to correlation effects [38]. The peaks values of G_K^{el} are of the order of a few 0.01 $k_B\Gamma$ ($k_B\Gamma$ is about 4.198×10^{-10} W/K for $\hbar\Gamma \simeq 20$ meV). Therefore, the peak values are smaller than the thermal conductance quantum $g_0(T) = \pi^2 k_B^2 T/(3h)$ at the room temperature $T = 1.25\hbar\Gamma \simeq 300$ K ($g_0(T) \simeq 9.456 \times 10^{-13}(W/K^2)T$) [67]. We point out that electron–vibration interactions affect the thermal conductance G_K^{el} in a way completely different from the charge conductance G (compare left upper and left lower panels of figure 5). Indeed, G_K^{el} gets enhanced with increasing the electron–oscillator coupling E_P. As discussed in the previous section, within the adiabatic approach, the molecular

effective level is renormalized by the position variable x which has a larger spreading upon increasing the electron–vibration coupling.

We stress that the behavior of the electron thermal conductance G_K^{el} shown in the lower left panel of figure 5 bears a strong resemblance with that of the phonon thermal conductance G_K^{ph} reported in figure 3. Both have a double-peak structure, and both are enhanced by the electron–vibration coupling. Moreover, G_K^{el} acquires values larger than those of G_K^{ph} in the energy region $-U \leqslant \epsilon \leqslant 0$. Obviously, the values of these quantities are comparable for the chosen value of phonon-induced damping rate $\gamma = 0.15\Gamma$. If one consider larger values of γ (for example $\gamma \simeq 0.4\Gamma$), then G_K^{ph} would play a major role in the total thermal conductance G_K. In any case, the values of G_K^{ph} and G_K^{el} differ for $\epsilon \gg 0$ and $\epsilon \ll -U$ since G_K^{ph} acquires a finite asymptotic value (obtained even in the absence of interactions on the molecule), while G_K^{el} goes rapidly to zero.

As shown in the lower right panel of figure 5, we analyze the behavior of the electronic thermoelectric figure of merit ZT^{el} neglecting the contribution from G_K^{ph}. The quantity ZT^{el} shows four peaks whose values are larger than 1, but smaller than the peak value around 3 obtained in the absence of interactions. We stress that the peak values of ZT^{el} at room temperature are almost coincident with the maxima and minima of the Seebeck coefficient S. Actually, close to room temperature, the small values of the conductance G are fully compensated by the large values of the Seebeck coefficient S. With increasing the electron–vibration coupling E_P, the reduction of G and S combines with the enhancement of G_K^{el} leading to a sensible reduction of the figure of merit ZT^{el}. Therefore, even if one neglects the role of phonon thermal conductance, the effect of electron–electron and electron–vibration interactions is able to induce a reduction of the figure of merit.

Before discussing the behavior of the total figure of merit ZT, we analyze the interplay between the Seebeck coefficient S and the charge conductance G. As shown in the upper panel of figure 6, in the spinless case, S is a decreasing function of G in the p-type window (S positive) apart from a small region close to zero conductance. On the other hand, S is an increasing function of G in the n-type window (S negative) excluding again a small range with vanishing conductance. In any case, the magnitude of the Seebeck coefficient S decreases with increasing the conductance G excluding a very small region. We note that this behavior is very similar to the results discussed in a recent work [68]. The electron–vibration coupling E_P does not change this behavior qualitatively. Indeed, not only the peak value of G is reduced, but also the maximum value of S gets decreased with increasing E_P. Only in the region with very low charge conductance do the curves for different values of E_P overlap.

As shown in the lower panel of figure 6, there is a splitting of the S versus G curve due to the double-peak structure observed in both conductance and Seebeck coefficient (see upper panel of figure 5). The large value of U affects more the conductance peak than the maxima of the Seebeck coefficient. Moreover, in analogy with the spinless case, the electron–vibration coupling E_P reduces each of the curves S versus G. As discussed in appendix B, with increasing U, the first minimum of S as a function of the energy ϵ becomes more negative, tending to get the same value in modulus (of the order of 3 K_B/e) of the first maximum. In a specular way, with increasing U, the second maximum of S as a function of the energy ϵ becomes more positive tending to a value close in modulus to the second minimum (essentially the value relative to the free case). Therefore, at a large fixed value of U, the two positive peak values of S shown in the lower panel of figure 6 for small G correspond to the two maxima of S, which have un equal heights. An analogous behavior is shown by the two negative peak values of S for small G. Therefore, the splitting of the S versus G curve is a fingerprint of finite strong electron–electron correlations. Clearly, in the limit $U \to \infty$ (in appendix B, $U = 40$ is close to this limit), the splitting would be absent, in analogy with the spinless case.

Finally, in figure 7, we focus on the total figure of merit ZT as a function of the level energy ϵ for different values of electron–vibration coupling E_P at $U = 20\hbar\Gamma$ including the effects of the phonon thermal conductance ($\gamma = 0.15\Gamma$). From the comparison with the results discussed in the previous paragraph, it emerges that the phonon thermal conductance G_K^{ph} induces an additional suppression of ZT. For the realistic value of $E_P = 0.5$ (intermediate coupling regime), the peak values of ZT are decreased by a factor of 2 in comparison with ZT^{el}, therefore the reduction of ZT is not strong. Only for unrealistically large electron–vibration couplings (E_P larger than 1), does ZT acquire peak values less than unity. Summarizing, the cooperative effects of phonon leads, electron–electron and electron–vibration interactions on the molecule are able to weaken the thermoelectric performance of this kind of device. However, within a realistic regime of parameters, the thermoelectric figure of merit ZT is still of the order of unity, making these devices a valid choice for thermoelectric applications.

5. Results within the non-linear response regime

In this section, we will discuss non-linear properties in analogy with the device model proposed in a recent paper [23]. Actually, the bias voltage V will be a free parameter, which will be adjusted together with other parameters in order to obtain a maximal efficiency of the device. In analogy with the cited paper [23], in this section, we will

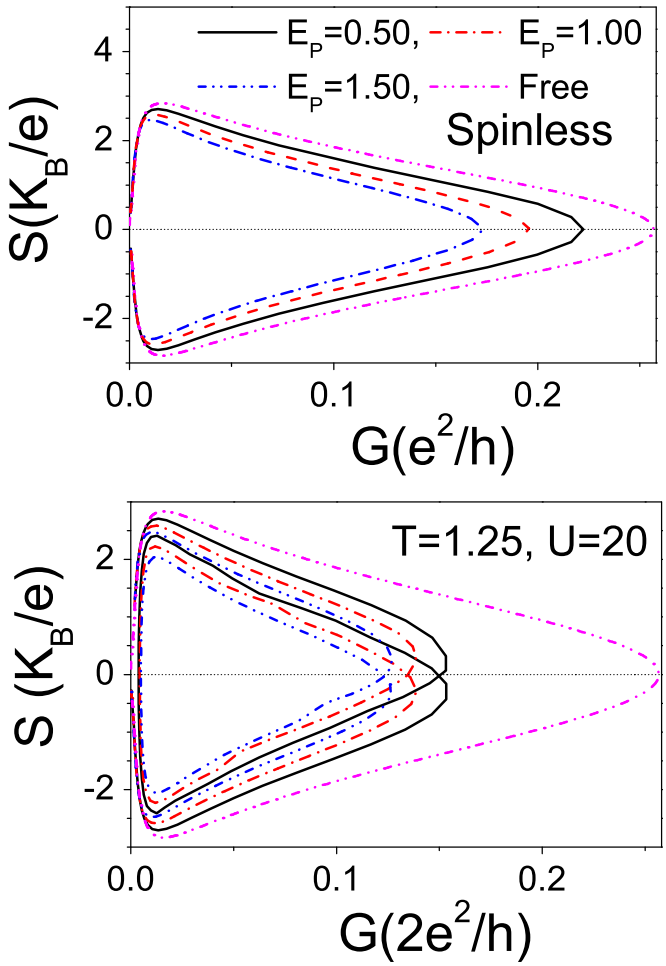

Figure 6. Seebeck coefficient S (in units of k_B/e) relative to the spinless case (upper panel) and to $U = 20\hbar\Gamma$ (lower panel) as a function of the electron conductance G (in units of $2e^2/h$) for different values of electron–vibration coupling E_P (in units of $\hbar\Gamma$). In all the plots, $T = 1.25\hbar\Gamma/k_B$ (close to room temperature).

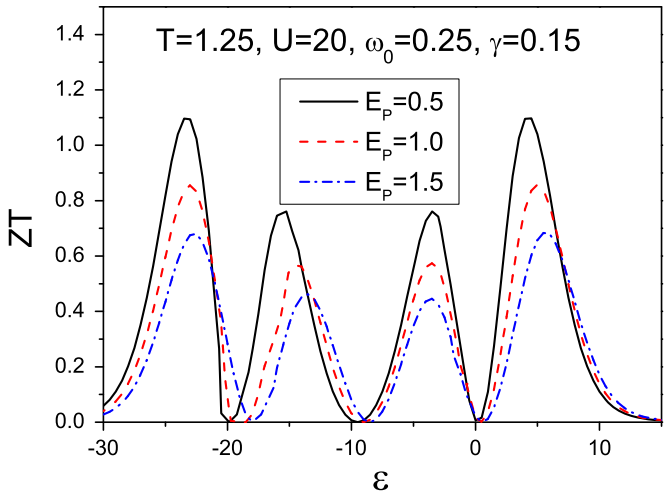

Figure 7. Dimensionless thermoelectric figure of merit ZT as a function of level energy ϵ (in units of $\hbar\Gamma$) for different values of electron–vibration coupling E_P (in units of $\hbar\Gamma$). In the plot, $U = 20\hbar\Gamma$, $T = 1.25\hbar\Gamma/k_B$, $\gamma = 0.15\Gamma$ and $\omega_0 = 0.25\Gamma$.

consider as parameters of the leads $\mu_L = 0$, $T_L = T + \Delta T$ (hot left lead), and $\mu_R = V$, $\mu_R = T$ (cold right lead). In any case, we will analyze the effects of a finite temperature difference ΔT and voltage V.

The problem of the stability of molecular junctions under large voltage bias and temperature difference is of particular relevance. Under voltage bias V, the effective vibrational temperature can be even 200 K larger than that at $V = 0$ [69]. Moreover, when current passes through fullerene junctions, the temperature before the decomposition of the C_{60} cage can be larger than 1000 K [70]. Therefore, experimental results suggest that large difference temperatures could be sustained by molecular junctions. In any case, in this paper, we will consider V up to $3\hbar\Gamma/e$ and ΔT up to $3\hbar\Gamma/k_B$ (of the order of 700 K).

We point out that, within the adiabatic approach, for stationary non-equilibrium states, electronic charge and energy currents are conserved within the numerical accuracy: $J^e = J^e_L = -J^e_R$, with J^e_α charge current from the α electron lead, and $J^{el} = J^{el}_L = -J^{el}_R$, with J^{el}_α energy current from the α electron lead. Putting together charge and energy currents, one can define the electron heat current $J^{eh}_\alpha = J^{el}_\alpha - (\mu_\alpha/e)J^e_\alpha$. Moreover, the phonon energy currents are conserved for generic nonequilibrium states within our accuracy: $J^{ph} = J^{ph}_L = -J^{ph}_R$, with J^{ph}_α energy (or heat) current from the α phonon lead. Therefore, within the adiabatic approach used in this paper, the conservation laws are satisfied within numerical accuracy since the charge current is conserved, and the energy currents are separately conserved for the electron and vibrational channels.

One can define the total heat current $J^{th}_\alpha = J^{eh}_\alpha + J^{ph}_\alpha$ from the α lead. We have checked that, within our numerical accuracy, the electric outer power $P = J^e V$ is equal to the total heat current $J^{th} = J^{th}_L + J^{th}_R$ (a result imposed by the first law of thermodynamics). For the device considered in this paper, the efficiency η is defined in terms of the heat current J^{th}_L flowing out of the hot left lead:

$$\eta = \frac{J^e V}{J^{th}_L}. \tag{24}$$

The efficiency can never exceed the Carnot value $\eta_{\rm Carnot}$

$$\eta_{\rm Carnot} = 1 - \frac{T}{T + \Delta T}, \tag{25}$$

therefore $\eta \leqslant \eta_{\rm Carnot}$. In the following, we will carefully analyze the behavior of the efficiency η by varying the parameters of the device model close to room temperature, focusing on the effects of many-body interactions and lead phonon–molecule coupling.

In figure 8, we show contour plots of the efficiency η as a function of the bias voltage V and of the electron level energy ϵ for different strengths of electron–vibration interaction: $E_P = 0.05$ (weak coupling, upper panel), $E_P = 0.25 = \hbar\omega_0$ (weak to intermediate coupling, lower panel). These plots are compatible with those appearing in the literature [23]. We point out that the maximal efficiency occurs for values of ϵ close to 5, a value where, as shown in figure 7, the thermoelectric figure of merit ZT shows a maximum. Therefore, there is a strong correlation between the behavior of ZT and η as a function of the level energy ϵ. On the other hand, the maxima of η take place at values of bias V which are not small (of the order of 1.5), in contrast with the behavior of ZT obtained in the linear response regime. Finally, the electron–vibration coupling E_P induces an overall sensitive reduction of the efficiency η. This trend is similar to the global decrease of ZT with increasing E_P shown in our recent paper [49].

In figure 9, we show contour plots of the efficiency η as a function of the bias voltage V and of the electron level energy ϵ for different strengths of lead phonon-molecule coupling: $\gamma = 0.01$ (very weak coupling, upper panel), $\gamma = 0.15$ (realistic coupling, middle panel), $\gamma = 0.4$ (very large coupling, lower panel). The position of maximal η does not change with increasing γ. However, the value of maximal η strongly decreases with increasing γ. Therefore, the efficiency η is strongly sensitive to the lead phonon-molecule coupling. Again the behaviors of the efficiency η and ZT can be joined.

The results discussed in figures 8 and 9 are relative to the temperature difference $\Delta T = 1$. In figure 10, we report the maximum of the efficiency, $\eta_{\rm MAX}$, as a function of ΔT for different values of lead phonon–molecule coupling: $\gamma = 0$ (black solid line with circles) and $\gamma = 0.15\Gamma$ (red solid line with squares). As expected, both efficiencies go to zero for small ΔT (behavior shared by the ideal Carnot efficiency $\eta_{\rm Carnot}$ shown in figure 10 as a dashed line). For $\gamma = 0$, η is smaller than $\eta_{\rm Carnot}$. Actually, η is about half of the Carnot limit (a reasonable value if $\gamma = 0$) in the regime of large ΔT. For $\gamma = 0.15$, η becomes slightly smaller than the efficiency for $\gamma = 0$, therefore, η is not negligible in comparison with the ideal Carnot limit for reasonable values of parameters within the regime of weak to intermediate electron–vibration and lead phonon–vibration coupling. In figure 10, we have added dotted lines on the curves for different values of vibration–lead phonon coupling. In particular we have considered lines passing through points between $\Delta T = 0$ and $\Delta T = 0.1$ (which in our units is about 25 K). We point out the decrease of the slopes with increasing γ. For comparison, in the figure, we have also included the tangent at the origin to the curve representing the Carnot efficiency $\eta_{\rm Carnot}$. Finally, we have considered the behavior of the ratio R between the maximal efficiency and the Carnot one. In the inset of figure 10, we report R

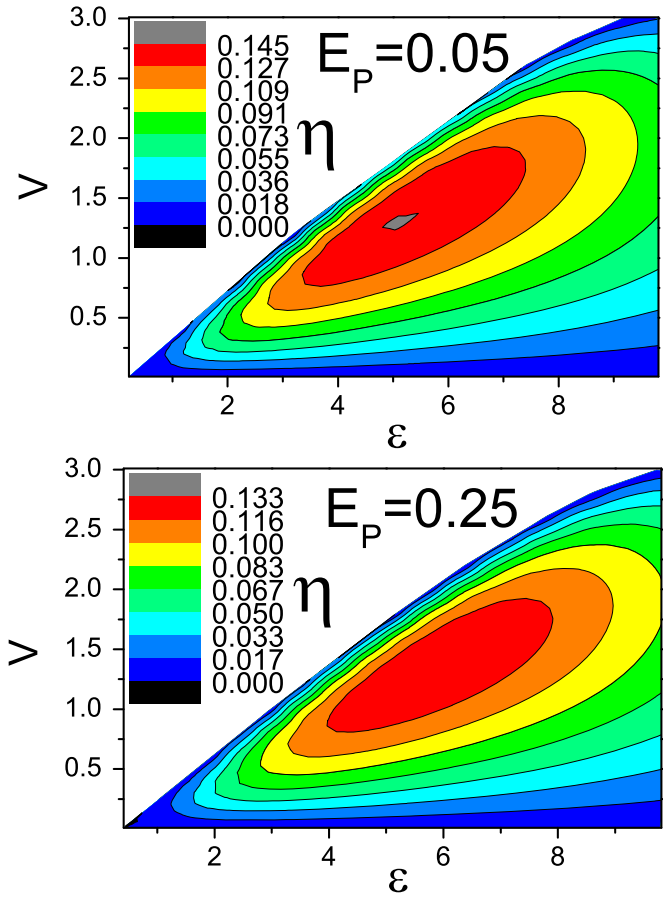

Figure 8. Upper panel: Contour plot of the efficiency η as a function of the bias voltage V (in units of $\hbar\Gamma/e$) and of the electron level energy ϵ (in units of $\hbar\Gamma$) for electron–vibration coupling $E_P = 0.05$ (in units of $\hbar\Gamma$). Lower panel: contour plot of the efficiency η as a function of the bias voltage V and of the electron level energy ϵ for electron–vibration coupling $E_P = 0.25$ (in units of $\hbar\Gamma$). In the plots, $U = 25\hbar\Gamma$, $T = 1.25\hbar\Gamma/k_B$ (close to room temperature), $\Delta T = \hbar\Gamma/k_B$, $\gamma = 0.15\Gamma$, and $\omega_0 = 0.25\Gamma$.

as a function of the temperature difference ΔT for different values of γ. In particular, in the range of small ΔT, R is about 0.35 for for $\gamma = 0$ and about 0.15 for for $\gamma = 0.15\Gamma$. Therefore, even in the regime of small efficiency, the ratio R is not negligible.

6. Conclusions

In this paper, the thermoelectric properties of a molecular junction have been studied within the linear and non-linear response regime at room temperature. The interplay between the low-frequency center of mass oscillation of the molecule and the electronic degrees of freedom has been investigated using a non-equilibrium adiabatic approach devised for including the large electron–electron Coulomb repulsion. Within the intermediate electron–vibration coupling regime, the phonon thermal conductance G_K^{ph} is quite sensitive to the changes in the occupation of electron level. Moreover, apart from an important asymptotic value (for $\epsilon \gg 1$), we have stressed that G_K^{ph} resembles the electron thermal conductance G_K^{el}. With increasing the electron–vibration coupling, the phonon and the electron thermal conductance get larger, while both the charge conductance G and the thermopower S get smaller. We have found that the figure of merit ZT depends appreciably on the behavior of G_K^{ph} and intramolecular interactions. Indeed, ZT can be substantially reduced, but its peak values can be still of the order of unity within the regime of weak to intermediate electron–vibration and lead phonon–vibration coupling. Finally, the efficiency η (evaluated within the non-linear response regime) can be correlated to the behavior of ZT (calculated within the linear response regime) as a function of the gate voltage, and, within the regime of weak to intermediate electron–vibration and lead phonon–vibration coupling, η is found to be slightly less than half of the Carnot limit for large temperature differences. We point out that, if at least one of the electron–vibration and phonon–vibration couplings becomes strong, the efficiency gets substantially reduced in comparison with the Carnot one.

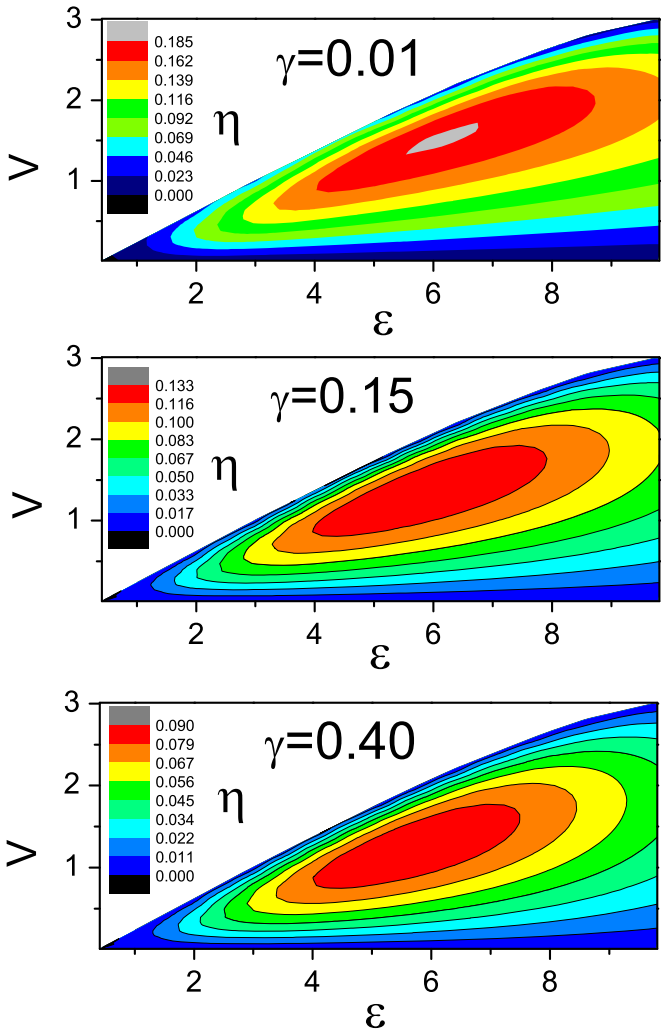

Figure 9. Upper panel: contour plot of the efficiency η as a function of the bias voltage V (in units of $\hbar\Gamma/e$) and of the electron level energy ϵ (in units of $\hbar\Gamma$) for lead phonon–molecule coupling $\gamma = 0.01\Gamma$. Middle panel: contour plot of the efficiency η as a function of the bias voltage V and of the electron level energy ϵ for lead phonon–molecule coupling $\gamma = 0.15\Gamma$. Lower panel: contour plot of the efficiency η as a function of the bias voltage V and of the electron level energy ϵ for lead phonon–molecule coupling $\gamma = 0.40\Gamma$. In the plots, $U = 25\hbar\Gamma$, $T = 1.25\hbar\Gamma/k_B$ (close to room temperature), $\Delta T = \hbar\Gamma/k_B$, $E_P = 0.25\hbar\Gamma$, and $\omega_0 = 0.25\Gamma$.

The parameters of the junction are determined by the coupling between molecule and metallic leads in the electronic and vibrational channels. For instance, the strength of the intramolecular couplings depends on the choice of the leads which screen the electron–electron and electron–vibration interactions. In order to improve the thermoelectric efficiency, molecules and metallic leads forming the junction have to ensure a weak phonon-center of mass coupling (small γ) and a small strength of the electron-center of mass interaction (small E_P). For realistic values of these couplings, the values of the phonon thermal conductance G_K are small compared to bulk conductances. Therefore, the values of ZT of the order of unity can be found in molecular junctions since these systems provide a mechanism to keep the phonon thermal conduction lower than that of bulks and other low-dimensional structures. Finally, in this paper, we have shown that, for realistic values of junction parameters, the phonon thermal conductance can be even smaller than the electron counterpart in a large range of gate voltages.

The electron–vibration interaction of the Anderson–Holstein model analyzed in this paper is related to the charge density injected by the external leads onto the molecule. The renormalization of the lead-molecule hopping integral induced by the center of mass movement could represent another possible source of electron–vibration coupling [22] and it can be studied within the adiabatic approach. However, we expect that the coupling through electron level density plays a major role due to the large mass of the molecules considered in this work. Finally, we stress that the approach proposed in this paper can be generalized to the study of more realistic multi-level molecular models and to cases where the number of atomic units within the molecule can be varied.

We emphasize that the focus of the paper has been on the steady-state dynamics of the system in the realistic regime of weak to intermediate electron–vibration coupling. The issue of the transient dynamics, which has

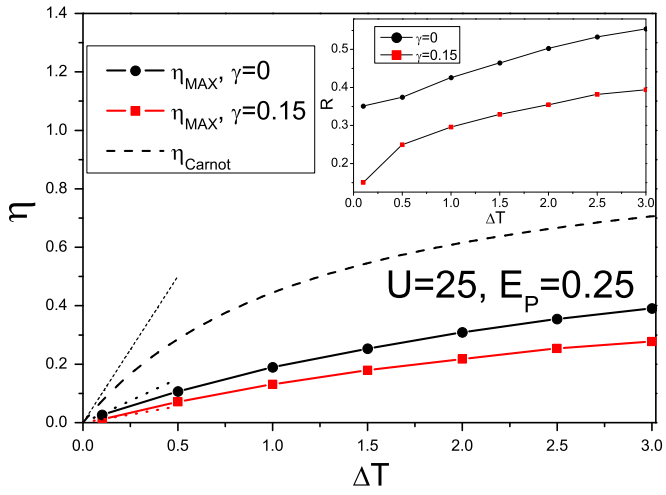

Figure 10. Maximal efficiency η_{MAX} as a function of the temperature difference ΔT (in units of $\hbar\Gamma/k_B$) for lead phonon-molecule coupling $\gamma = 0$ (black solid line with circles), and $\gamma = 0.15\Gamma$ (red solid line with squares). In the plot, $U = 25\hbar\Gamma$, $T = 1.25\hbar\Gamma/k_B$ (close to room temperature), $E_P = 0.25\Gamma$ and $\omega_0 = 0.25\Gamma$. For comparison, the Carnot efficiency η_{Carnot} is shown as dashed line. The dotted lines highlight the slopes in the regime of small ΔT. In the inset, the ratio R between the maximal efficiency and the Carnot efficiency for $\gamma = 0$ (solid line with black circles), and $\gamma = 0.15\Gamma$ (solid line with red squares).

recently attracted the interest of many researchers [71–75], has not been addressed. Some work on the transient regime in the presence of a temperature difference between the leads is in progress. In any case, within the weak to intermediate electron–vibration coupling regime analyzed in this paper, the oscillator dynamics does not involve very long transients, which, however, are typically present in the strong electron–vibration regime. Actually, in this last regime, the oscillator potential can be characterized by a double well with high barriers between the minima. The oscillator potentials analyzed in this paper do not show such features.

Acknowledgments

This work has been performed in the frame of the project GREEN (PON02 00029 2791179) granted to IMAST S. c.a.r.l. and funded by the MIUR (Ministero dell'Istruzione, dell'Università e della Ricerca).

Appendix A. Comparison between different approaches within the Coulomb blockade regime

In this appendix, we compare the approach used in the main text for strong Coulomb repulsion with that of Lacroix [76] which retains additional self-energy corrections upon the atomic limit [50]. We will consider the electronic properties in the absence of electron–vibration coupling since we are interested only on the effects induced by the electron–electron interaction in equilibrium conditions at temperature $T = T_\alpha$ and chemical potential $\mu = 0 = \mu_\alpha$. In this appendix, we will use the same units of the main text.

In contrast with the main text, in this appendix, we will use a slightly different kind of wide-band approximation for the electron leads. Actually, we will consider an energy-dependent tunneling rate $\Gamma_0(E) = \Gamma$, for $-E_c \leqslant E \leqslant E_C$, and zero elsewhere, with E_C cutoff energy much larger than U. Therefore, the retarded self-energy of the electron level $\Sigma_0(E)$ due to the effects of the electron leads is

$$\Sigma_0(E) = \Lambda_0(E) - \frac{i}{2}\Gamma_0(E), \tag{A.1}$$

where $\Lambda_0(E)$ is the real part of the retarded self-energy

$$\Lambda_0(E) = \int_{-\infty}^{+\infty} \frac{dE'}{2\pi} \frac{\Gamma_0(E')}{E - E' + \mu} = \frac{\Gamma}{2\pi} \ln \left| \frac{E - E_C + \mu}{E + E_C + \mu} \right|. \tag{A.2}$$

In the limit where $E_C \to \infty$, one recovers the wide band approximation used in the main text corresponding to a zero real part $\Lambda_0(E)$.

We focus on the retarded Green function $G_L^R(\omega)$ relative to the paramagnetic solution in order to calculate the spectral function $A_L(\omega) = -2\Im G_L^R(\omega)$. The retarded Green function within the Lacroix approximation for large U [50, 76] is

$$G_L^R(\omega) = \frac{1-\rho}{\hbar\omega - \epsilon - \Sigma_0(\hbar\omega) - \Sigma_h(\hbar\omega)} + \frac{\rho}{\hbar\omega - \epsilon - U - \Sigma_0(\hbar\omega) - \Sigma_p(\hbar\omega)}, \tag{A.3}$$

where ρ is the level density per spin self-consistently calculated through the following integral

$$\rho = \int_{-\infty}^{+\infty} \frac{\mathrm{d}(\hbar\omega)}{2\pi i} G_L^<(\omega), \tag{A.4}$$

with the equilibrium lesser Green function $G_L^<(\omega)$

$$G_L^<(\omega) = i f(\hbar\omega) A_L(\omega), \tag{A.5}$$

and $f(\hbar\omega) = 1/(\exp[\beta(\hbar\omega - \mu)] + 1)$ is the free Fermi distribution corresponding to the average chemical potential $\mu = 0$. In equation (A.3), the self-energy $\Sigma_h(\hbar\omega)$ is

$$\Sigma_h(\hbar\omega) = -\frac{U\Sigma_1(\hbar\omega)}{\hbar\omega - \epsilon - U - \Sigma_0(\hbar\omega) - \Sigma_3(\hbar\omega)}, \tag{A.6}$$

while the self-energy $\Sigma_p(\hbar\omega)$ is

$$\Sigma_h(\hbar\omega) = \frac{U\Sigma_2(\hbar\omega)}{\hbar\omega - \epsilon - \Sigma_0(\hbar\omega) - \Sigma_3(\hbar\omega)}, \tag{A.7}$$

where the self-energy $\Sigma_i(\hbar\omega)$, with $i = 1, 2, 3$, is given by

$$\Sigma_i(\hbar\omega) = \int_{-\infty}^{+\infty} \frac{\mathrm{d}E}{2\pi} \Gamma_i(E) \times \left[\frac{1}{\hbar\omega + E - \mu - 2\epsilon - U + i\eta} + \frac{1}{\hbar\omega - E + \mu + i\eta} \right], \tag{A.8}$$

with $\Gamma_1(E) = \Gamma_0(E) f(E)$, $\Gamma_2(E) = \Gamma_0(E)[1 - f(E)]$, $\Gamma_3(E) = \Gamma_0(E)$, and $\eta \to 0^+$. We notice that, for large U, the weights of the poles of the Green function in equation (A.3) are the same of the Green function examined in the main text. The Green function within the Lacroix approach has the additional self-energy terms $\Sigma_i(\hbar\omega)$, which take into account tunneling processes back and forth to the leads.

As shown in figure A1 , we compare the spectral function obtained within the approach used in the main text and A_L within the Lacroix approximation [76] close to room temperature for two values of U ($U = 40$ upper panel, $U = 16$ lower panel). Both spectral functions exhibit a bimodal structure whose peaks are separated by the energy U. The positions of the peaks within the two approaches are very close, while the heights of the peaks are slightly different. However, the ratio of the spectral weights of the two peaks does not significantly depend on the approach. Obviously, the modification of the isolated resonances is slightly more complicated within the Lacroix approach than that due to the self-energy $\Sigma_0(\hbar\omega)$ alone. Actually, the peaks within the Lacroix approach tend to be a little bit asymmetric. Summarizing, the differences between the two approaches are minimal, supporting the use of the Green function method adopted in the present work. Finally, the small differences between the two approaches are quantitatively similar with decreasing U from 40 to 16.

In this appendix, we also analyze the total level occupation $N = 2\rho$ (within the paramagnetic solution). This quantity has been calculated by the two approaches discussed in this appendix, finding minimal differences. In figure A2 , we report the occupation determined by the approach used in the main text as a function of level energy ϵ for different values of U. It shows the typical profiles of the Coulomb blockade. Actually, for level energy ϵ around $-U/2$, N is 1. The energy region with occupation close to 1 gets enhanced with increasing the value of U. Moreover, for ϵ around $\mu = 0$, N goes from 1 to 0, while, for ϵ around $-U$, there is the transition from $N = 2$ to $N = 1$. These particular values of ϵ are carefully analyzed in the main text when the effects of the electron–vibration coupling are included.

Appendix B. Transport properties for different values of the Hubbard interaction U

In this appendix, we analyze the transport properties for different values of the Hubbard interaction U.

First, as reported in figure B1 , we analyze the effects of the Hubbard interaction U on the electronic response functions as a function of the level energy ϵ at a fixed value of electron–vibration coupling E_P ($E_P = 0.25$) in the absence of coupling to phonon leads ($\gamma = 0$) close to room temperature ($T = 1.25$). For comparison, we report the transport properties relative to the case when electron–electron and electron–vibration interactions are neglected (indicated as 'Free' in the figure).

As shown in the upper left panel of figure B1, close to room temperature, the charge conductance G is smaller than the free one due to the effects of interactions. Moreover, G has maxima for $\epsilon \simeq 0 = \mu$ and $\epsilon \simeq -U$,

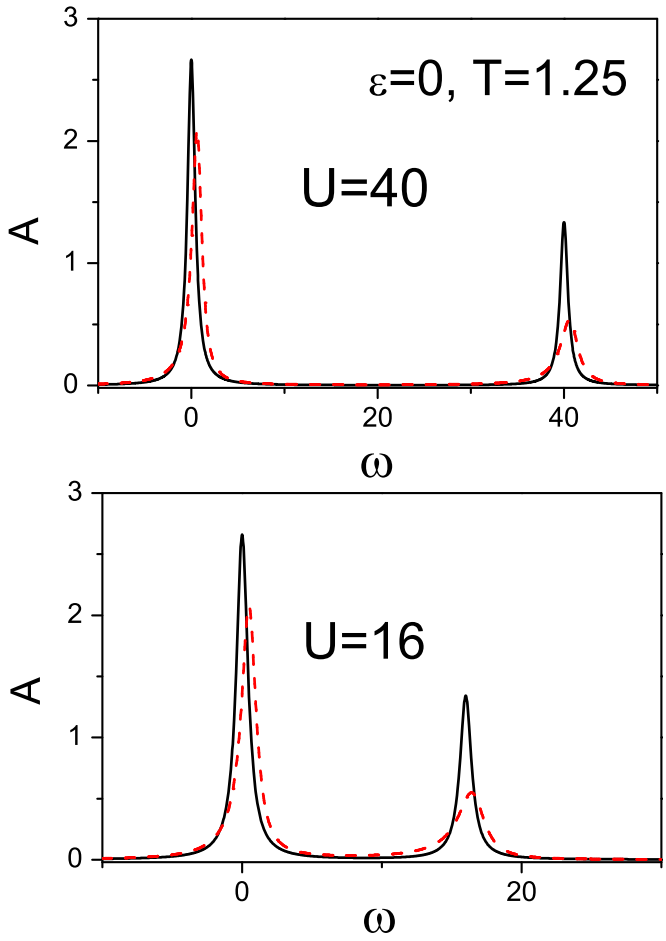

Figure A1. Spectral function A (in units of $1/\hbar\Gamma$) as a function of frequency ω (in units of Γ) for Hubbard interaction $U = 40\hbar\Gamma$ (upper panel) and $U = 16\hbar\Gamma$ (lower panel) at level energy $\epsilon = 0$ and $T = 1.25\hbar\Gamma/k_B$ (close to room temperature) in the absence of electron–vibration coupling. Solid line: first correction upon the atomic limit (used in the main text); dashed line: additional correction upon the atomic limit (Lacroix approach).

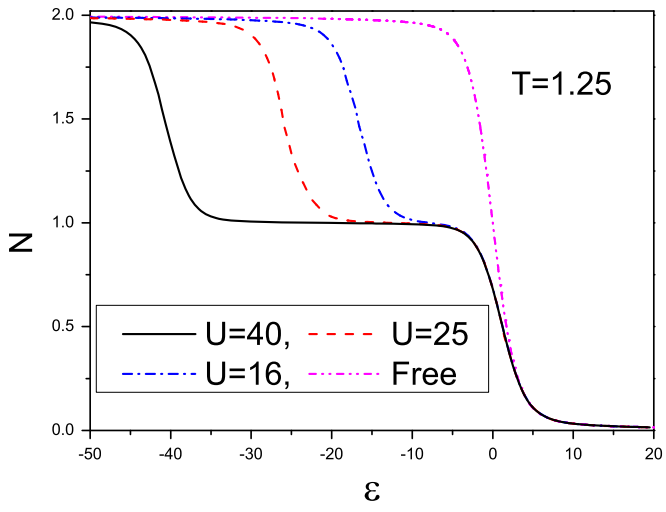

Figure A2. Level density N as a function of level energy ϵ (in units of $\hbar\Gamma$) for different values of the Hubbard interaction U (in units of $\hbar\Gamma$) at $T = 1.25\hbar\Gamma/k_B$ (close to room temperature) in the absence of electron–vibration coupling.

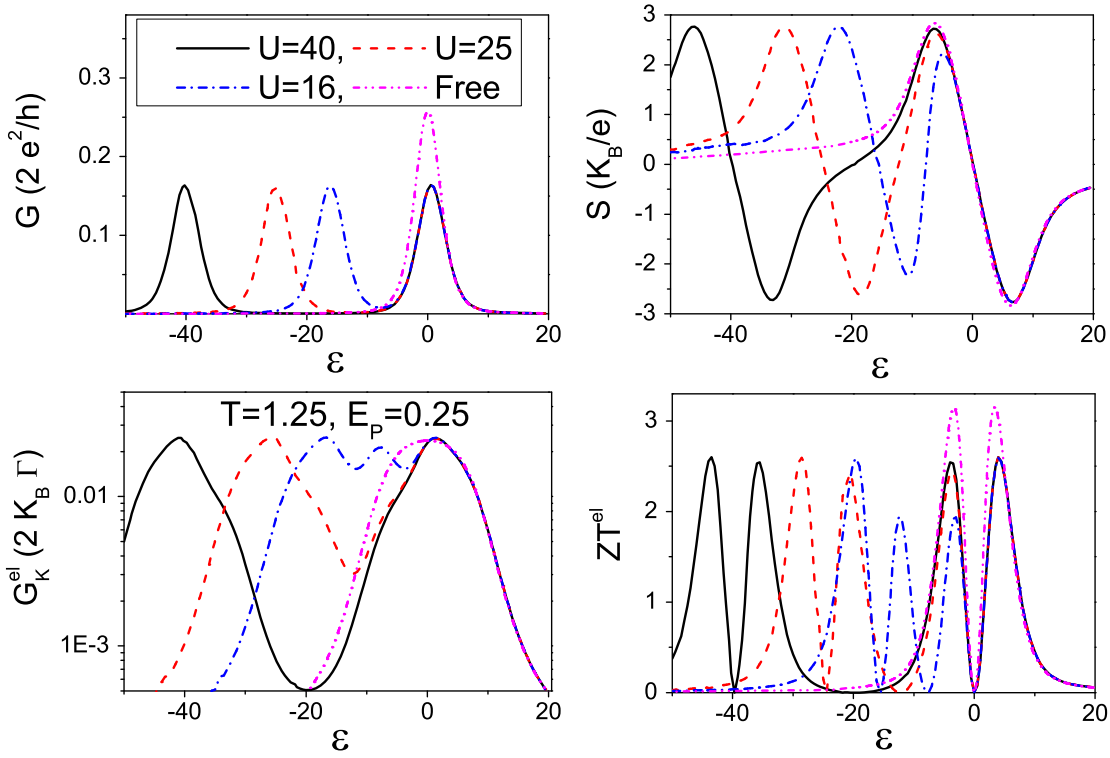

Figure B1. Electron conductance G in units of $2e^2/h$ (upper left panel), Seebeck coefficient S in units of k_B/e (upper right panel), electron thermal conductance G_K^{el} in units of $2k_B\Gamma$ (lower left panel), and electronic figure of merit ZT^{el} (lower right panel) as a function of the level energy ϵ (in units of $\hbar\Gamma$) for different values of Hubbard interaction U (in units of $\hbar\Gamma$). In all the plots, $E_P = 0.25\hbar\Gamma$, $\gamma = 0$, and $T = 1.25\hbar\Gamma/k_B$ (close to room temperature).

and a minimum at $\epsilon \simeq -U/2$. Therefore, the position of the first peak shows a strong sensitivity to the changes of the values of U, while the heights of the two peaks are nearly constant.

As shown in the upper right panel of figure B1, the first maximum and minimum of the Seebeck coefficient S show large position variations with changing U. Actually, the structure close to $\epsilon = 0$ (where S vanishes) is nearly translated by $-U$. Therefore, even at $\epsilon \simeq -U/2$, S gets very small values. Indeed, strong electron correlations induce a complex behavior in S. In particular, with increasing U, the first minimum becomes more negative tending to get the same value in the modulus (of the order of 3 K_B/e) of the first maximum. A similar behavior is shown by the second maximum of S, whose height increases as a function of U.

As shown in the lower left panel of figure B1, with varying the level energy ϵ, the electron thermal conductance G_K^{el} shows the characteristic correlation-induced double-peak structure similar to that of the charge conductance. In contrast with the behavior of the conductance, the values between the maxima are strongly decreasing with increasing U giving rise to a minimum of G_K^{el}.

Finally, as shown in the lower right panel of figure B1, we analyze the behavior of the electronic thermoelectric figure of merit ZT^{el} neglecting the contribution from G_K^{ph}. As a result of the behavior of the previous transport quantities, the first two peaks of ZT^{el} show positions dependent on the Hubbard strength U. Since the peak values of ZT^{el} at room temperature are almost coincident with the maxima and minima of the Seebeck coefficient S, the second peak of ZT^{el} (corresponding to the first minimum of S) increases its value with increasing U. Therefore, the effect of large electron–electron interactions is able to induce changes of the figure of merit.

As reported in the upper panel of figure B2 , the behavior of the phonon thermal conductance G_K^{ph} bears a a strong resemblance with that of the electron thermal conductance G_K^{el} shown in the lower left panel of figure B1. Both have a double-peak structure, whose first maximum has an energy position corresponding to about $\epsilon \simeq -U$. Moreover, the peak values of these two quantities are comparable for the chosen value of phonon-induced damping rate $\gamma = 0.15\Gamma$. However, for large and small ϵ, G_K^{ph} is characterized by an asymptotic value which corresponds to the contribution given by the only phonon leads neglecting the effects of electron–electron and electron–vibration interactions on the molecule. On the other hand, for $\epsilon \simeq -U/2$, G_K^{ph} is poorly influenced by the electron–electron effects, getting values close to the asymptotic one.

Finally, as reported in the lower panel of figure B2, we focus on the total figure of merit ZT as a function of the level energy ϵ for different values of electron–electron Hubbard interaction U at fixed value of the electron–

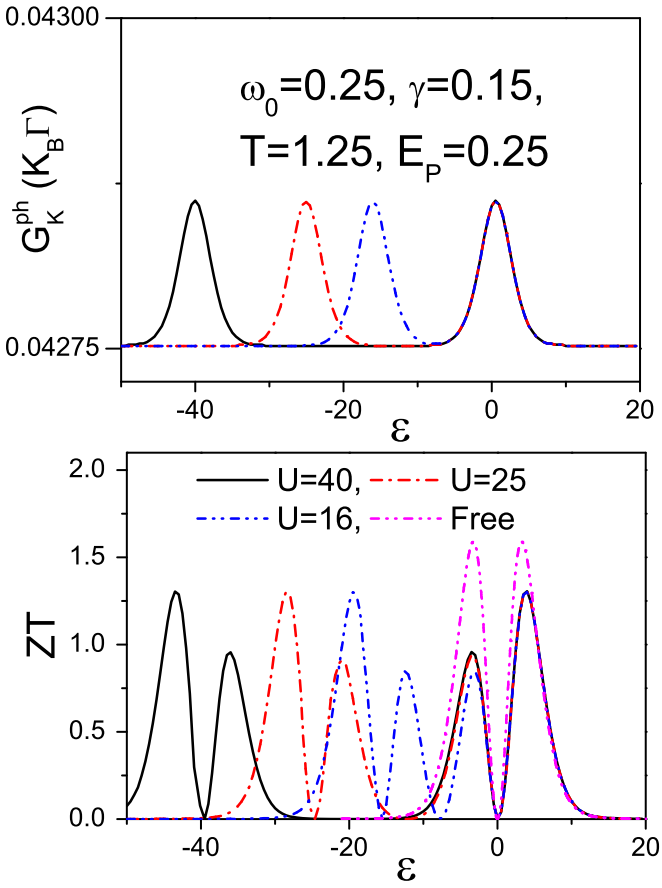

Figure B2. Phonon thermal conductance G_K^{ph} in units of $k_B\Gamma$ (upper panel) and thermoelectric figure of merit ZT (lower panel) as a function of level energy ϵ (in units of $\hbar\Gamma$) for different values of the Hubbard interaction U (in units of $\hbar\Gamma$) at $T = 1.25\hbar\Gamma/k_B$ (close to room temperature). In all the plots, $E_P = 0.25\hbar\Gamma$, $\omega_0 = 0.25\hbar\Gamma$, and $\gamma = 0.15\hbar\Gamma$.

vibration coupling E_P including the effects of the phonon thermal conductance ($\gamma = 0.15\Gamma$). From the comparison with the electronic figure of merit reported in the lower right panel of figure B1, the phonon thermal conductance G_K^{ph} induces an additional suppression of ZT, but it does not shift the peaks.

References

[1] Nolas G S, Sharp J and Goldsmid J 2001 *Thermoelectrics: Basic Principles and New Materials Developments* (Berlin: Springer)
[2] Ioffe A F 1957 *Semiconductor Thermoelements and Thermoelectric Cooling* (London: Infosearch Limited)
[3] Kittel C 2004 *Introduction to Solid State Physics* (New York: Wiley)
[4] Shakouri A 2011 *Annu. Rev. Mater. Res.* **41** 399
[5] Biswas K, He J, Blum I D, Wu C-I, Hogan T P, Seidman D N, Dravid V P and Kanatzidis M G 2012 *Nature* **489** 414
[6] Koumoto K and Mori T 2013 *Thermoelectric Nanomaterials — Materials Design and Applications* (Berlin: Springer)
[7] Sothmann B, Sanchez R and Jordan A N 2015 *Nanotechnology* **26** 032001
[8] Venkatasubramanian R, Siivola E, Colpitts T and O'Quinn B 2001 *Nature* **413** 597
[9] Harman T C, Taylor P J, Walsh M P and LaForge B E 2002 *Science* **297** 2229
[10] Hochbaum A I, Chen R, Delgado R D, Liang W, Garnett E C, Najarian M, Majumdar A and Yang P 2008 *Nature* **451** 163
[11] Hicks L D and Dresselhaus M S 1993 *Phys. Rev.* B **47** 16631
[12] Murphy P G and Moore J E 2007 *Phys. Rev.* B **76** 155313
[13] Venkatasubramanian R 2001 *Recent Trends in Thermoelectric Materials Research III Semiconductors and Semimetals* vol 71 (New York: Academic Press) 175–201
Chen G 2001 *Recent Trends in Thermoelectric Materials Research III Semiconductors and Semimetals* vol 71 (New York: Academic Press) 203–59
[14] Mahan G D and Sofo J 1996 *Proc. Natl Acad. Sci. USA* **93** 7436
[15] Aradhya S V and Venkataraman L 2013 *Nat. Nanotechnol* **8** 399
[16] Dubi Y and di Ventra M 2011 *Rev. Mod. Phys.* **83** 131
[17] Reddy P, Jang S-Y, Segalman R A and Majumdar A 2007 *Science* **315** 1568
[18] Yee S K, Malen J A, Majumdar A and Segalman R A 2011 *Nano Lett.* **11** 4089
[19] Finch C M, Garcia-Suarez V M and Lambert C J 2009 *Phys. Rev.* B **79** 033405
[20] Murphy P, Mukerjee S and Moore J 2008 *Phys. Rev.* B **78** 161406(R)
[21] Galperin M, Nitzan A and Ratner M A 2008 *Mol. Phys.* **106** 397
[22] Koch J, von Oppen F, Oreg Y and Sela E 2004 *Phys. Rev.* B **70** 195107

[23] Leijnse M, Wegewijs M R and Flensberg K 2010 *Phys. Rev.* B **82** 045412
[24] Paulsson M and Datta S 2003 *Phys. Rev.* B **67** 241403(R)
[25] Cuevas J C and Scheer E 2010 *Molecular Electronics: An Introduction to Theory and Experiment* (Singapore: World Scientific)
[26] Datta S 2012 *Lessons from Nanoelectronics: A New Perspective on Transport* (Singapore: World Scientific)
[27] Wang R Y, Segalman R A and Majumdar A 2006 *Appl. Phys. Lett.* **89** 173113
[28] Wang Z, Carter J A, Lagutchev A, Koh Y K, Seong N-H, Cahill D G and Dlott D D 2007 *Science* **317** 787
[29] Meier T, Menges F, Nirmalraj P, Hölscher H, Riel H and Gotsmann B 2014 *Phys. Rev. Lett.* **113** 060801
[30] Lee W, Kim K, Jeong W, Zotti L A, Pauly F, Cuevas J C and Reddy P 2013 *Nature* **498** 209
[31] Schoeps V, Zlatic V and Costi T A 2011 *J. Phys.: Conf. Ser.* **273** 012155
[32] Galperin M, Nitzan A and Ratner M A 2007 *J. Phys. Condens.: Matter* **19** 103201
[33] Park H, Park J, Lim A K L, Anderson E H, Alivisatos A P and McEuen P L 2000 *Nature* **407** 57
[34] Qin H, Holleitner A W, Eberl K and Blick R H 2001 *Phys. Rev.* B **64** 241302(R)
[35] Yang K-H, Zhao Y-L, Wu Y-J and Wu Y-P 2010 *Phys. Lett.* A **374** 2874
[36] Zianni X 2010 *Phys. Rev.* B **82** 165302
[37] Entin-Wohlman O, Imry Y and Aharony A 2010 *Phys. Rev.* B **82** 115314
[38] Liu J, Sun Q-F and Xie X C 2010 *Phys. Rev.* B **81** 245323
[39] Ren J, Zhu J-X, Gubernatis J E, Wang C and Li B 2012 *Phys. Rev.* B **85** 155443
[40] Bagheri Tagani M and Rahimpour Soleimani H 2013 *Physica* B **413** 86
[41] Arrachea L, Bode N and von Oppen F 2014 *Phys. Rev.* B **90** 125450
[42] Hsu B C, Chiang C-W and Chen Y-C 2012 *Nanotechnology* **23** 275401
[43] Remaggi F, Traverso Ziani N, Dolcetto G, Cavaliere F and Sassetti M 2013 *New J. Phys.* **15** 083016
Traverso Ziani N, Piovano G, Cavaliere F and Sassetti M 2011 *Phys. Rev.* B **83** 245311
[44] Mozyrsky D, Hastings M B and Martin I 2006 *Phys. Rev.* B **73** 035104
[45] Pistolesi F, Blanter Ya M and Martin I 2008 *Phys. Rev.* B **78** 085127
[46] Hussein R, Metelmann A, Zedler P and Brandes T 2010 *Phys. Rev.* B **82** 165406
[47] Nocera A, Perroni C A, Marigliano Ramaglia V and Cataudella V 2011 *Phys. Rev.* B **83** 115420
[48] Nocera A, Perroni C A, Marigliano Ramaglia V and Cataudella V 2012 *Phys. Rev.* B **86** 035420
[49] Perroni C A, Ninno D and Cataudella V 2014 *Phys. Rev.* B **90** 125421
[50] Haug H and Jauho A-P 2008 *Quantum Kinetics in Transport and Optics of Semiconductors* (Berlin: Springer)
[51] Weiss U 2008 *Quantum Dissipative Systems* (Singapore: World Scientific)
[52] Burkle M, Hellmuth T J, Pauly F and Asai Y 2015 *Phys. Rev.* B **91** 165419
[53] Markussen T 2013 *J. Chem. Phys.* **139** 244101
[54] Lu X, Grobis M, Khoo K H, Louie S G and Crommie M F 2003 *Phys. Rev. Lett.* **90** 096802
[55] Yu L H and Natelson D 2005 *Nano Lett.* **4** 79
[56] Mravlje J, Ramsak A and Rejec T 2006 *Phys. Rev.* B **74** 205320
[57] Schiró M and le Hur K 2014 *Phys. Rev.* B **89** 195127
[58] Perroni C A, Cataudella V, de Filippis G and Marigliano Ramaglia V 2005 *Phys. Rev.* B **71** 113107
[59] Splettstoesser J, Governale M, König J and Fazio R 2005 *Phys. Rev. Lett.* **95** 246803
[60] Hernández A R, Pinheiro F A, Lewenkopf C H and Mucciolo E R 2009 *Phys. Rev.* B **80** 115311
[61] Nocera A, Perroni C A, Marigliano Ramaglia V, Cantele G and Cataudella V 2013 *Phys. Rev.* B **87** 155435
[62] Perroni C A, Nocera A and Cataudella V 2013 *Europhys. Lett.* **103** 58001
[63] Perroni C A, Romeo F, Nocera A, Marigliano Ramaglia V, Citro R and Cataudella V 2014 *J. Phys.: Condens. Matter* **26** 365301
[64] Honeycutt R L 1992 *Phys. Rev.* A **45** 600
[65] Honeycutt R L 1992 *Phys. Rev.* A **45** 604
[66] Wang J-S 2007 *Phys. Rev. Lett.* **99** 160601
[67] Jezouin S, Parmentier F D, Anthore A, Gennser U, Cavanna A, Jin Y and Pierre F 2013 *Science* **342** 601
[68] Jeong C, Kim R, Luisier M, Datta S and Lundstrom M 2010 *J. Appl. Phys.* **107** 023707
[69] Ward D R, Corley D A, Tour J M and Natelson D 2011 *Nat. Nanotechnol* **6** 33
[70] Schulze G, Franke K J, Gagliardi A, Romano G, Lin C S, Rosa A L, Niehaus T A, Frauenheim T, di Carlo A, Pecchia A and Pascual J I 2008 *Phys. Rev. Lett.* **100** 136801
[71] Riwar R P and Schmidt T L 2009 *Phys. Rev.* B **80** 125109
[72] Tahir M and MacKinnon A 2010 *Phys. Rev.* B **81** 195444
[73] Wilner E Y, Wang H, Cohen G, Thoss M and Rabani E 2013 *Phys. Rev.* B **88** 045137
[74] Albrecht K F, Martin-Rodero A, Monreal R C, Muhlbacher L and Levy Yeyati A 2013 *Phys. Rev.* B **87** 085127
[75] Biggio M, Cavaliere F, Storace M and Sassetti M 2014 *Ann. Phy.* **526** 541
[76] Lacroix C 1981 *J. Phys.* F **11** 2389